LLNL-PROC-675114
APS / Shock Cmprssn. Cndnsd. Matter, Tampa, FL, June 14-19, 2015

Speckle-adaptive VISAR Fringe Analysis Technique

David Erskine[1,a)]

[1]*L-487, Lawrence Livermore Nat. Lab., Livermore, CA 94550, USA*

[a)]Corresponding author: erskine1@llnl.gov

Abstract. A line-VISAR (velocity interferometer) is an important diagnostic in shock physics, simultaneously measuring many fringe histories of adjacent portions of a target splayed along a line on a target, with fringes recorded vs time and space by a streak camera. Due to laser speckle the reflected intensity may be uneven spatially, and due to irregularities in the streak camera electron optics the phase along the slit may be slightly nonlinear. Conventional fringe analysis algorithms which do not properly model these variations can suffer from inferred velocity errors. A speckle-adaptive algorithm has been developed which senses the interferometer and illumination parameters for each individual row (spatial position Y) of the 2d interferogram, so that the interferogram can be compensated for Y-dependent nonfringing intensity, fringe visibility, and nonlinear phase distribution. In numerical simulations and on actual data we have found this individual row-by-row modeling improves the accuracy of the result, compared to a conventional column-by-column analysis approach.

INTRODUCTION

The VISAR velocity interferometer[1, 2, 3] is an important diagnostic for shock physics and equation of state (EOS) experiments, that measures the time history of Doppler shifted light reflected from shock or ramp loaded targets. Various algorithms for converting streak camera interferogram fringes to a complex signal $\mathbf{W}(t)$ (i.e. phase and magnitude) are popular, including an FFT method[4], a sine fit along a column, and push-pull treatment of four rows at 90 degrees[2, 5]. (The article Ref. 6 on line-imaging velocimetry, section on data reduction, is a good review.)

Here we describe an algorithm, called "Speckle Adaptive", which we have developed and used over the last few years which distinguishes itself from conventionally used interferogram analysis algorithms by being able to sense and then correct for irregular and unknown illumination intensity and interferometer phase versus position Y along the streak camera slit. (Hence the term "speckle" here is a bit more general and refers to irregularities not only in illumination but in phase.) Such irregularities in illumination can come from coherent nature of laser illumination. An example is shown in Fig. 1(a) for rows Y=18 and 32. Irregularities in phase can come from nonlinearities in the electron optics of a streak camera, acting upon the intended linear splaying of interferometer phase with position along the slit by tilting an interferometer mirror.

These irregularities can cause errors in the perceived science fringe phase. For intensity variations that are similar to a fringe period along the Y-direction, they can distort the science fringe phase with a polarity that depends on which side of the science fringe it overlays. Since the science fringe position usually changes, this results in a velocity error that tends to form a wiggle in time.

The new algorithm has also been used by this author in processing astronomical dispersed interferometer data for high resolution spectroscopy and the Doppler exoplanet search, called externally dispersed interferometry[7], where illumination could vary vs phase step by the passing of clouds or speckle of atmospheric turbulence, and where phase steps were unknown and irregular due to possible air convection or mechanical vibration in the interferometer combined with the wavelength spanning a wide bandwidth (phase step is reciprocal to wavelength for a given interferometer mirror displacement). For the astronomical spectroscopic application the horizontal variable in the interferogram is wavelength or wavenumber, instead of time.

There are applications for this algorithm in interferometric metrology where air convection or mechanical vibrations can create uncertainty of phase steps, while the effect being measured is unchanged.

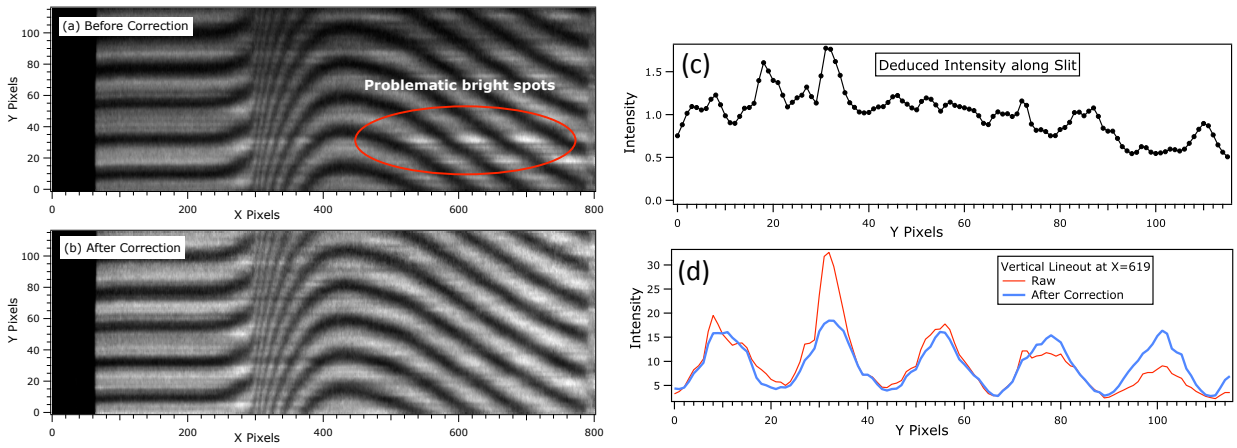

FIGURE 1. Streak camera VISAR interferogram data, before (a) and after (b) correction for uneven illumination intensity profile along slit (Y-direction), deduced from data by method of projections (so that it is not confused by mixture of nonfringing and fringing components). Bright spots in uncorrected data at X~600, Y~30 are due to speckle nature of laser illumination. Deduced profile (c) is used to divide interferogram to produce (b), and blue curve of (d). This yields a more accurate fringe phase history. Shot s52238 by Ray Smith.

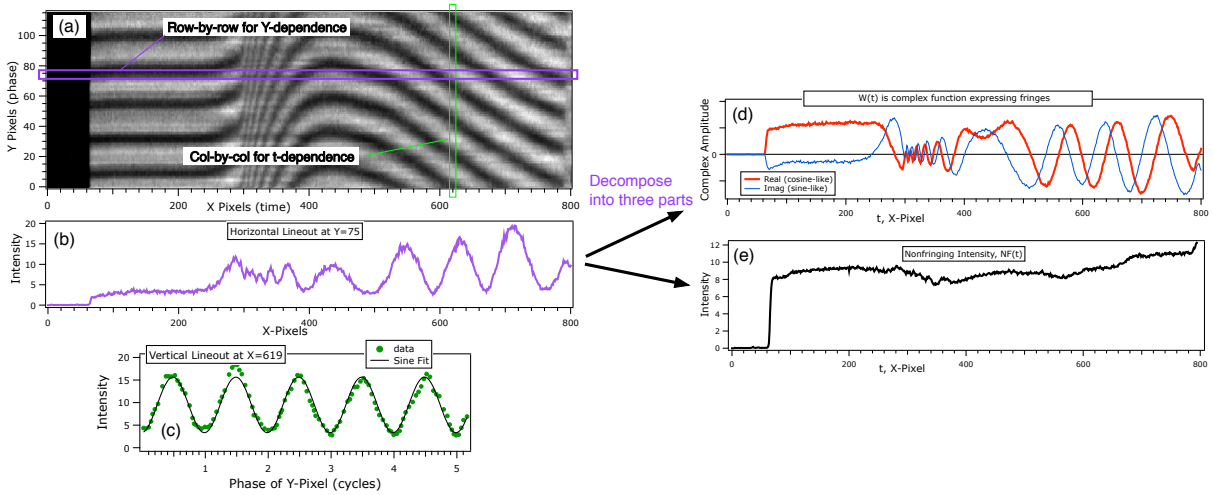

FIGURE 2. The algorithm iterates between column-by-column and row-by-row processing. The col-by-col processing finds the time-dependence of the nonfringing $NF(t)$ (e), and two fringing (d) templates Re $\mathbf{W}(t)$ and Imag $\mathbf{W}(t)$, which is also the science results. The row-by-row processing finds how much of each of three templates resides in a given horizontal lineout (b), for each Y. The amount of NF vs Y measures the intensity spatial variation $Slit(y)$, and the polar angle of $\mathbf{W}(t)$ measures the phase $\phi(y)$.

This technique will work best when there are enough wiggles vs time in the fringes that they can be distinguished from the nonfringing signal (i.e. illumination times target reflectivity), meaning that an overlap integral between the fringing terms and the nonfringing terms (over some time region which could be a subset of the total record) should be smaller than any of the self-overlap integrals. The technique will work for records having a decaying portion behind a shock, or a ramp compression, when the amount of phase change is at least a half fringe or so. It will not work well for purely discontinuous shocks that do not have a decaying portion behind the shock, since in that case the fringing and nonfringing signals look similar, being step functions.

In the simplest implementation presented here, we assume that the speckle is steady in time (defining a horizontal region), and that the underlying velocity profile (physics), manifested in $\mathbf{W}(t)$, is a global function independent of Y over the rows being used (defining a vertical region). However, the local magnitude (Mag_y) and phase (ϕ_y) of the fringes for a given row is expected to vary with Y, (the phase usually varies approximately linearly). If one defines a local Y-dependent $\mathbf{W}_y(t)$ to describe the fringe component of a given row, it would be related to the global $\mathbf{W}(t)$ via

$$\mathbf{W}_y(t) = Mag_y \; e^{i2\pi\phi_y} \; \mathbf{W}(t) \tag{1}$$

and there would also be a nonfringing Y-dependent component $\mathrm{NF}_y(t)$, also called $Slit_y$.

In order to measure Y-dependence of the velocity history, such as commonly found in targets subjected to tilted impacts or the effect of side release waves, one performs a loop over the entire Y-region where the velocity history for each increment of Y inside the loop is found for a relatively small Y-region. The minimum Y-region over which any algorithm can practically work is 2/3 of a cycle of phase, since a minimum of 3 points is needed to define a sinusoid when the period is fixed, but we commonly use 1 cycle of phase in our loops. However, for brevity the math treatment in this report assumes there is no Y-dependence to the velocity history (physics) manifested in $\mathbf{W}(t)$.

Iterate Between Finding Time and Spatial Dependence

Figure 2 and Figure 3 show that the algorithm alternates between looping through the 2d data in a column-by-column basis (to find the time dependence) and a row-by-row basis (to find the Y dependence). A conventional algorithm, such as Fourier Transform Method (FTM)[4], would perform only a column-by-column process and make assumptions about the spatial dependence of the illumination and phase (usually that they are uniform and linear with Y, respectively). Whereas with the new algorithm we add an important step where we sense, for each row, what is the reflected illumination intensity and phase. We do this by decomposing the lineout along a row into three components, a nonfringing component NF(t) and two fringing components, Re $\mathbf{W}(t)$ and Imag $\mathbf{W}(t)$. The amplitudes of these components tell us the reflected nonfringing intensity $Slit_y$ and phase ϕ_y representing each row. (A later section describes details of the decomposition process.) Then we can normalize the 2d data by this slit function $Slit_y$ and process it in the column-by-column approach to yield a better estimate of the time-dependence. Since the column-by-column and row-by-row processes depend on each others outputs for inputs, we obviously iterate between the two. Figure 4 describes our column-by-column process, which differs from the conventional by being able to handle irregular phases, whereas the FTM implicitly requires evenly spaced data in phase.

Note that the starting condition of $Slit_y = 1$ and linear phase for the iteration is essentially equivalent to using the FTM method, so the very first estimate of $NF(t)$ and $\mathbf{W}(t)$ will be close to the conventional result. For every iteration after that, the estimate of $NF(t)$ and $\mathbf{W}(t)$ should improve upon the conventional result since it is using improved information about the illumination and phase spatial dependence. This can only help.

Our algorithm returns the detected phase vs Y, and it is usually approximately linear. We use any instance of it having grossly nonlinear character as a diagnostic to alert us that the algorithm is not converging properly, or that there is a pathology in the data for a given row. In that case, we adjust our Y-region to avoid that row, and it usually fixes the problem.

We find that for well behaved data (meaning uniform illumination) we obtain virtually the same result as the conventional algorithm, but for "problem child" data which has weak and irregular appearing fringes, we often are able to obtain cleaner looking velocity results than the conventional method. Figure 5 shows example raw and corrected image data (normalized by $Slit_y$), and Figure 6 the extracted velocities for an omega shot s75263 obtained by Amy Lazicki. Comparison to velocities using the conventional method shows our method improves upon it, particularly in the early time period 0.8 to 2.5 ns, where the two independently processed VISARs (red, blue curves) looking at same target agree better, between themselves, than for the conventional pair (black, gray curves). Our results also include ghost fringe subtraction using a new method (described in another paper of this conference[8]), and so are an integral demonstration of our total processing pipeline.

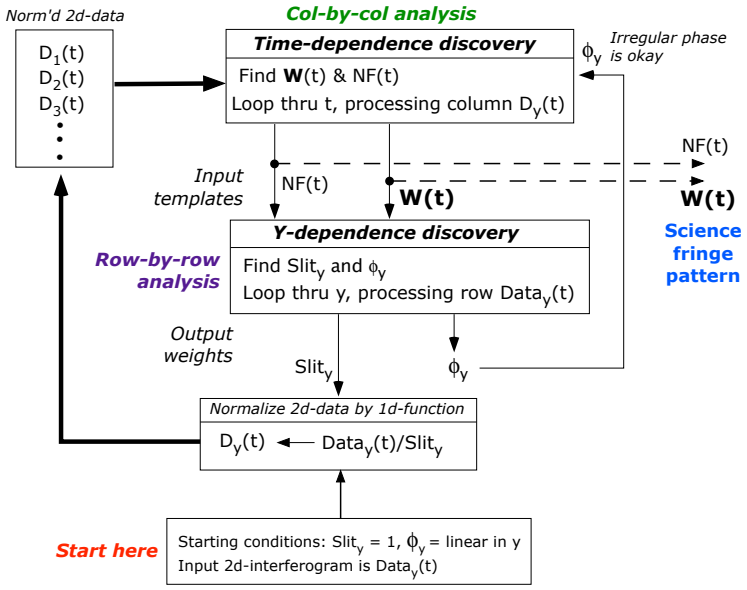

FIGURE 3. Flowchart of the iterative procedure. The starting condition of uniform intensity ($Slit_y = 1$) and linear phase ϕ_y produces the same results as a conventional algorithm. Hence at the first iteration we achieve the conventional result for $\mathbf{W}(t)$. After that we measure the Y-dependence of the illumination and phase, which can improve the result for next calculation of $\mathbf{W}(t)$.

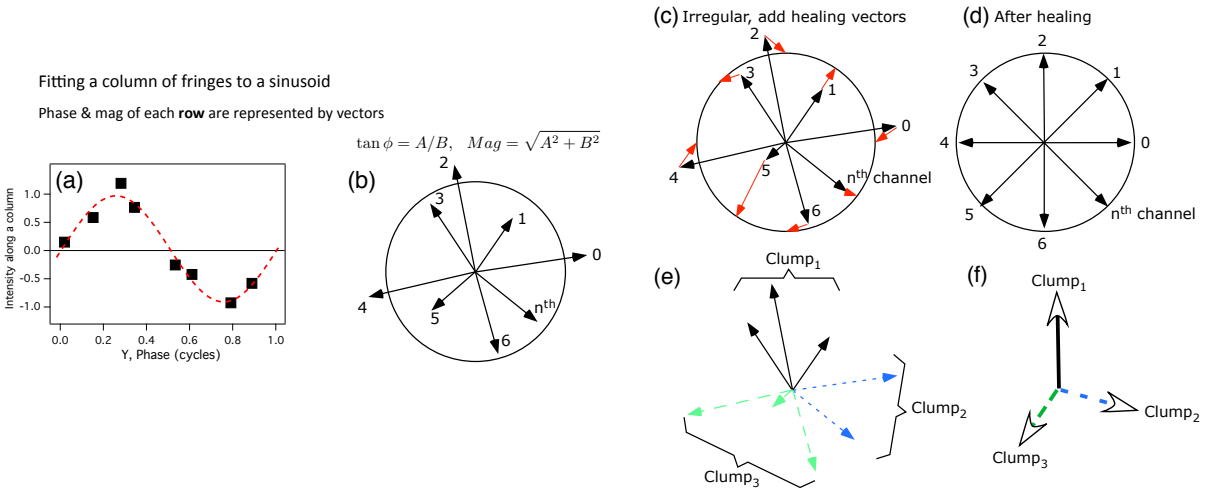

FIGURE 4. The steps in the column-by-column analysis that finds $NF(t)$ and $\mathbf{W}(t)$ for a given t, anticipating that the phase and fringe magnitude could be irregular, but are known (by the row-by-row process). The fitting of data to a sinusoid (a) having irregular phase can be represented by vectors (b) that represent the row and whose phase and magnitude are computed from the coefficients B, C, from the projection math. The irregular vectors are converted to a regular arrangement by adding or subtracting any combination of other vectors of the set, provided the nonfringing signal has already been subtracted so that only a sinusoidal component remains. The "healing" vectors (red, in panel c) needed to bring the irregular vectors into regularity (d) are assembled from mixtures of three clump vectors (e)(f), which are groups of data, so that weak data naturally does not add much noise to the final result. The regular set of vectors (d) at uniformly spaced angles ϕ'_y becomes a Fourier evaluation through $\mathbf{W} = \Sigma e^{i2\pi\phi'_y} D(y)$ of a column $D_y(t)$.

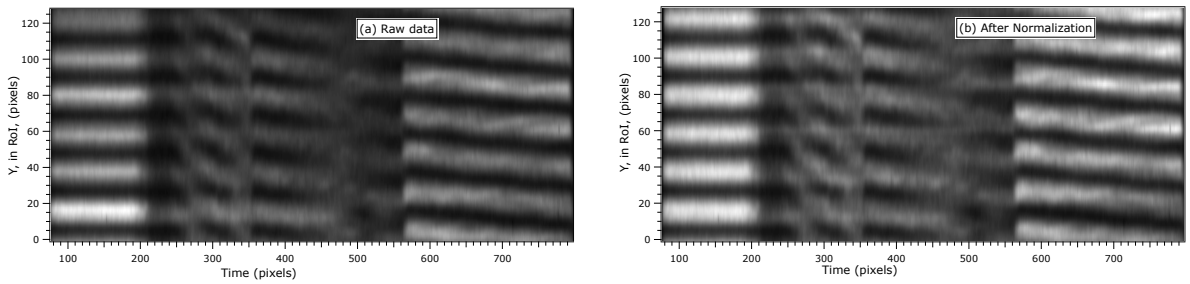

FIGURE 5. VISAR #2 interferogram data of Omega shot s75263, before (a) and after (b) normalization by *Slit*(*y*), when the algorithm senses the amount of nonfringing intensity in each row Y of the data. Note the more vertically uniform intensities of (b). The center of the six cycle (128 Y-pixel) region of interest shown is from Y=500 in the original data. Velocities obtained from this data, after ghost subtraction, are shown in Fig. 6. This is data on Qz/LiF/Qz obtained by Amy Lazicki.

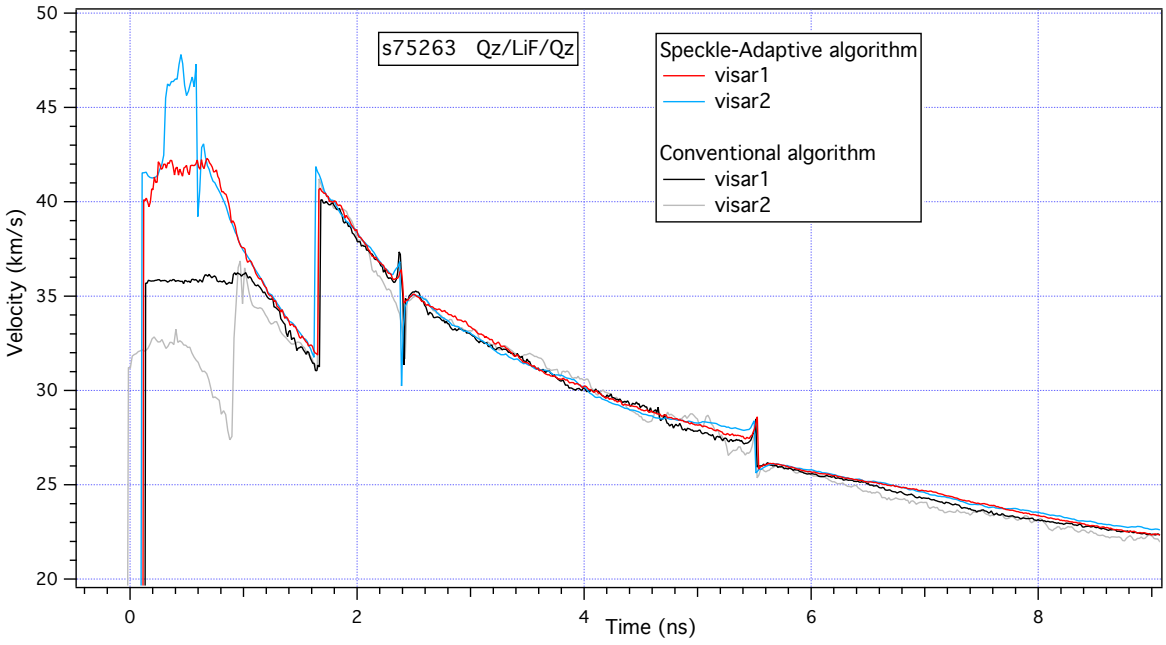

FIGURE 6. Velocity histories of the data of Fig. 5 (Qz/LiF/Qz Omega shot s75263 by Amy Lazicki) processed by the Speckle Adaptive (red, blue) and conventional (black, gray) techniques, for two VISARs used in parallel having different velocity per fringe proportionalities (visar #1, red and black, has more fringes per velocity unit). Ghost fringe analyses were also done using different methods, so this is an integral demonstration. See other paper of this conference for this author's method of Ghost artifact removal[8].

Finding the Y-dependence: Projection Method

We suppose we have provisional knowledge of the time dependence of the fringe $\mathbf{W}(t)$ and nonfringing *NF(t)* components, (also called templates or basis functions), and we are given a row Y of intensity data $D_y(t)$, and we want to learn the amplitudes of these components. We express $\mathbf{W}(t)$ in its real and imaginary parts, also called cosine-like and sine-like parts, $F_c(t) + iF_s(t) \equiv \mathbf{W}(t)$. We have the linear equation

$$D_y(t) = a_y F_s(t) + b_y F_c(t) + c_y F_{NF}(t) \tag{2}$$

and we will solve for the coefficients a_y, b_y, and c_y, (where to promote the symmetry of the equations we relabel $c_y \equiv Slit_y$ & $F_{NF} \equiv NF$). From these we will get the row's phase and magnitude through

$$\tan 2\pi\phi_y = a_y/b_y \tag{3}$$

$$|W_{fringing}| = \sqrt{a_y^2 + b_y^2} \tag{4}$$

This magnitude and phase will be the length and direction of a vector (i.e. a complex value), called a designating vector, one for each row of intensity data (as in Fig. 4). The rule is, whatever manipulations (adding, subtracting, magnifying etc) that we perform on the designating vector, we also perform on the data row it represents.

To solve for the coefficients, we use a method of projections (overlap integrals) to generate from Eq. 2 a set of equations, equal in number to the number of terms (3) of Eq. 2. This set can then be directly solved by standard matrix methods (e.g. Cramer's rule using determinants). (These equations are similar to those obtained from doing a least squares minimization approach to the problem.) Let the overlap integral between two template functions $F_1(t)$ and $F_2(t)$ be represented by the more compact expression

$$\langle F_1 F_2 \rangle \equiv \int F_1(t) F_2(t) dt \tag{5}$$

where we choose the time region of the integration to include at least some portion of the time region prior to the shock, in order to measure the phase corresponding zero velocity in order to subtract it from the final result for velocity. In principle, if the speckle variation appears to change with time, then one could consider subdividing the analysis into different time regions within which the speckle is consistent. (If the velocity changes continuously one is allowed to match phases on either side.) But we have not done so yet– we have integrated over the entire record length.

To both sides of Eq. 2 we apply the overlap integral, three times using each of the template functions $F_c(t)$, $F_s(t)$, and *NF(t)*. This creates three linear equations:

$$\langle F_c D_y \rangle = a_y \langle F_c F_s \rangle + b_y \langle F_c F_c \rangle + c_y \langle F_c F_{NF} \rangle \tag{6}$$

$$\langle F_s D_y \rangle = a_y \langle F_s F_s \rangle + b_y \langle F_s F_c \rangle + c_y \langle F_s F_{NF} \rangle \tag{7}$$

$$\langle F_{NF} D_y \rangle = a_y \langle F_{NF} F_s \rangle + b_n \langle F_{NF} F_c \rangle + c_y \langle F_{NF} F_{NF} \rangle \tag{8}$$

The overlap integrals are quickly computed into values, and the three equations easily solved by Cramer's rule to yield the a_y, b_y, and c_y coefficients. Then we apply Eq. 2 to yield channel phase ϕ_y, and c_y is our slit intensity profile.

This decomposition process is least sensitive to noise if the three templates are approximately orthogonal, meaning the cross-overlap is smaller than the self-overlap $\langle F_1 F_2 \rangle < \langle F_1 F_1 \rangle$ etc, and we assume we have normalized magnitudes of the templates. Approximate orthogonality is easily achieved when the phase changes contiguously for at least a cycle, since it is rare for $NF(t)$ to have a similar looking sinusoidal wiggle. However, for step-function shapes such as from clean shocks without following pressure decays, this will be violated.

Finding the Time Dependence: Vector Healing Method

If one could assume the interferometer phase ϕ_y remains linear with y, i.e. not significantly distorted by the streak camera imaging, then one could use any of conventional interferogram fringe analysis algorithms to produce $\mathbf{W}(t)$ and *NF(t)*, such as FTM, which implicitly requires linear phase distribution of its data. And for some streak camera installations this may be a reasonable assumption.

However, we have developed a more general algorithm that can handle unknown and irregular distribution of phase steps, so that we do not worry about a requirement of linear phase. The first step is to subtract the measured amount of $NF_y(t)$ from each of the row data $D_y(t)$,

$$D_y(t) - c_y NF_y(t) \rightarrow D'_y(t) \tag{9}$$

so that the remaining signal is purely fringing, i.e. purely sinusoidal. This is necessary for the next section where we regularize a set of irregular vectors.

Regularization is simplest when the data consists purely of a sinusoidal term, so that every row belongs to the set of data which satisfies the requirement of sinusoidal behavior. In that case we are allowed to add any combination of other rows to it (to form a weighted sum), and it will retain its vector quality, because a sinusoid plus a sinusoid remains a sinusoid.

By analogy, consider the linear interpolation that we all commonly employ to recreate a missing data point in a curve (sequence of data points) that is approximately linear. To form the missing or corrected data point we compute a weighted sum of the two data points that bracket the gap, because each of those two satisfy the (physics) conditions that define the data. In principle, that weighted sum could also include other data further away from the immediate two bracketing data points. It is up to the user which points to use, and there are many possible solutions.

Instead of a linear interpolation, we use what could be called a sinusoidal interpolation to correct the irregular data and bring it into regularity. Figure 4 shows how we intelligently add amounts of other vectors to modify their direction and length (and do the same operations for the underlying row data). We call this process "healing".

We use a programmatically simple way of choosing the healing vectors and their weightings, by grouping vectors into clumps so that weak data is naturally weighted weakly. (Because there are many more elements of data than degrees of freedom, there is a myriad of possible ways to combine data. Other weighting schemes may be more optimal, and the optimal weighting depends on the nature of the noise, whether it depends on the signal intensity or not.)

Once the vectors are regularized, the column data can be processed by any of the conventional methods. We use a simple Fourier expression for each time column

$$\mathbf{W} = \Sigma e^{i2\pi\phi'_y} D'_y \tag{10}$$

where we use the regularized phases ϕ'_y which are evenly arranged around one cycle.

ACKNOWLEDGMENTS

Thanks to Amy Lazicki and Ray Smith for Omega VISAR data. Prepared by LLNL under Contract DE-AC52-07NA27344.

REFERENCES

[1] L. Barker and K. Schuler, J. Appl. Phys. **45**, 3692–3693 (1974).
[2] W. Hemsing, Rev. Sci. Instr. **50**, 73–78 (1979).
[3] D. Dolan, Sandia National Laboratory Tech. Rep. **SAND2006-1950** (2006).
[4] M. Takeda, H. Ina, and S. Kobayashi, Journal of the Optical Society of America (1917-1983) **72**, p. 156 January (1982).
[5] W. M. Trott, M. D. Knudson, L. C. Chhabildas, and J. R. Asay, "Measurements of spatially resolved velocity variations in shock compressed heterogeneous materials using a line-imaging velocity interferometer," in *American Institute of Physics Conference Series*, American Institute of Physics Conference Series, Vol. 505 (2000), pp. 993–998.
[6] P. M. Celliers, D. K. Bradley, G. W. Collins, D. G. Hicks, T. R. Boehly, and W. J. Armstrong, Review of Scientific Instruments **75**, 4916–4929 November (2004).
[7] D. J. Erskine, J. Edelstein, M. Sirk, E. Wishnow, Y. Ishikawa, E. McDonald, and W. V. Shourt, "High Resolution Broad-Band Spectroscopy in the NIR Using the TripleSpec Externally Dispersed Interferometer at the Hale Telescope," in *Ground-based and Airborne Instrumentation V*, Proc. SPIE, Vol. 9147 (2014) p. 914717.
[8] D. J. Erskine, "Ghost Fringe Removal Techniques Using Lissajous Data Presentation", AIP Conf. Series, 19th APS Topical Conf. Shock Cmprssn. Cndsd. Matter, Tampa, FL, June 14-19, 2015, paper W1.00069.